Electro-osmotic flow over a charged superhydrophobic surface

Hui Zhao*
Department of Mechanical Engineering, University of Nevada, Las Vegas, Nevada 89154, USA
(Received 18 March 2010; published 23 June 2010)

Bubbles can be trapped inside textured structures such as grooves, forming a superhydrophobic surface. A superhydrophobic surface has a large effective hydrodynamic slip length compared to a smooth hydrophobic surface and holds the promise of enhancing electrokinetic flows that find many interesting applications in microfluidics. However, recent theoretical studies suggested that electro-osmotic flows over a weakly charged superhydrophobic surface [the zeta potential of the surface is smaller than the thermal potential (25 mV)] can only be enhanced when liquid-gas interfaces are charged [T. M. Squires, Phys. Fluids **20**, 092105 (2008); Bahga *et al.*, J. Fluid Mech. **644**, 245 (2010)]. So far there is little work reported when the zeta potential of the surface is comparable or even larger than the thermal potential. In this paper we numerically investigate electro-osmotic flows over a periodically striped slip-stick surface by solving the standard Poisson-Nernst-Planck equations. Our results indicate that at large zeta potentials, even if liquid-gas interfaces are charged, the nonuniform surface conduction due to the mismatch between surface conductions over no-shear and no-slip regions leads to electric field lines penetrating the double layer and thus the nonuniform surface conduction weakens the tangential component of the electric field which primarily drives electro-osmotic flows. Our results imply that, in the presence of strong nonuniform surface conduction, enhanced electro-osmotic flows over a superhydrophobic surface are possible only in certain conditions. In particular, the enhancement due to the slip can potentially be lost at large zeta potentials. Similar loss of the enhancement of a charged particle's electrophoretic mobility due to the slip was reported by Khair and Squires [Phys. Fluids **21**, 042001 (2009)].

DOI: 10.1103/PhysRevE.81.066314 PACS number(s): 47.65.−d, 47.57.jd, 83.50.Rp, 47.61.Jd

I. INTRODUCTION

With the advance of nanofabrication and microfabrication technologies and novel, sensitive, and high-resolution experimental techniques, hydrodynamic slip over a smooth liquid-solid interface has been detected in experiments and slip length was measured to be about on the order of nanometers [1–7]. Since the hydrodynamic slip can reduce drags and enhance flow rates, it attracts more attention [2,6,8]. However, the enhancement due to the slip for a pressure-driven flow is determined by the ratio of the slip length to the height of the channel [9]. Thus, observed nanometer slip can only slightly enhance a pressure-driven flow for microfluidic applications.

To overcome the limitation of nanometer slip lengths over a smooth hydrophobic surface, the so-called superhydrophobic surfaces have great potential [8]. Superhydrophobic surfaces were inspired by the unique water-repellent properties of the lotus leaf [10]. These surfaces are covered with microstructures and nanostructures such as posts, grooves, or holes that can effectively trap bubbles. If the liquid surface is restricted to the top of the roughness (Cassie state) [8], the liquid will be in contact with the solid over a fraction of the surface, while the rest will be exposed to the gas phase with nearly zero viscosity [11,12]. The liquid moves over trapped bubbles with a significant reduction in friction, providing a means to boost the flow. With desired textured patterns, an apparent slip length of orders of microns over a superhydrophobic surface was observed [13–15]. A number of experimental and numerical studies have been conducted to investigate pressure-driven flows over superhydrophobic surfaces and to estimate apparent slip lengths [16–29].

Due to favorable scaling with miniaturization, electrokinetic phenomena have attracted increased interests and find various new applications in lab-on-a-chip devices and other emerging technologies [30,31]. One important application of electrokinetic flows is to drive and pump liquid in a small confined space [32]. Because the effect of the hydrodynamic slip for electro-osmotic (EO) flows is determined by the ratio of the slip length to the double layer thickness, it is possible to significantly enhance electrokinetic flows over a hydrophobic surface even for slip lengths of nanometers due to the fact that a typical double layer length is on the order of nanometers [33–38]. EO flows over a hydrophobic surface have many potential applications ranging from drag reduction [39,40], nanoscale energy conversion [41,42], to electrochromatography [43]. Further studies were also devoted to investigating the effect of the hydrodynamic slip on the electrophoretic mobility and the dipole moment [44,45].

Consider that the effective slip length of a superhydrophobic surface is much larger than the one of a traditional hydrophobic surface. One might intuitively expect that the combination of EO flows and a superhydrophobic surface might further massively amplify the induced flow. However, such giant amplification is not apparent since the effects of both slip lengths and surface charge distribution on a superhydrophobic surface are not homogeneous. The anisotropic nature of a superhydrophobic surface might adversely affect the enhancement of EO flows. In fact, Squires [46] studied EO flows over an inhomogeneously charged slipping surface in the limits of thin double layers and small zeta potentials and found that when the liquid-gas interface carries no charge, the EO flow is precisely the same as that over a homogeneously charged no-slip surface. In addition, Bahga

*hui.zhao@unlv.edu

et al. [47] derived analytical solutions of EO flows over a weakly charged superhydrophobic surface (small zeta potentials) and concluded that, for an arbitrary double layer thickness, there is no flow enhancement when the liquid-gas interface is uncharged and only significant flow enhancement is possible with charged liquid-gas interfaces.

Both Squires [46] and Bahga *et al.* [47] are restricted to small zeta potentials. At small zeta potentials, the nonuniform surface conduction over a superhydrophobic surface is negligible. But at moderate or large zeta potentials, as pointed out by Squires [46], the mismatch between surface conductions over no-shear regions and no-slip regions causes ions to exchange between the double layer and the bulk in order to maintain global ion conservation. This transport process deforms the electric field to penetrate the double layer. In other words, the tangential electric field driving EO flows is weakened due to this exchange, potentially leading to a reduction in EO flows. So far the consequence of the nonuniform surface conduction at large zeta potentials on flow enhancement has not been systematically studied yet. Moreover, ion transport between the double layer and the bulk creates a bulk concentration gradient outside the double layer [48]. This induced concentration gradient can generate an osmotic pressure difference that will drive a diffusio-osmotic flow [49]. Such a flow might also affect EO flows over a superhydrophobic surface.

In this paper, we will numerically investigate the role of the nonuniform surface conduction over a superhydrophobic surface in enhancing EO flows. The paper is organized as follows. The mathematical model is introduced in Sec. II. In Sec. III, we solve the proposed mathematical model with a regular perturbation expansion in terms of the applied electric field. In Sec. IV, we compare our numerical simulations with theoretical predictions in the limit of small zeta potentials. In Sec. V, we discuss the EO mobility characterizing the magnitude of electrokinetic flows in terms of zeta potentials of both no-shear and no-slip regions. Section VI concludes.

II. MATHEMATICAL MODEL

Consider a liquid flowing in a two-dimensional microchannel of a height $2H$ that contains periodically slip-stick strips. The no-shear regions are transverse to the flow direction. The width of the no-slip region is L_{NS} and the width of the no-shear region is L_S. Here, let $H=L_{NS}+L_S$. The channel is filled with a 1-1 symmetric electrolyte with permittivity ε_1. A uniform external electric field E_0 is imposed along the axial direction. Zeta potentials of no-slip and no-shear regions are, respectively, ζ_{NS} and ζ_S. Accordingly, electric double layers are developed near charged surfaces [50,51]. The external electric field drives excess ions inside the double layer to migrate, drag water to move with them, and induce an electro-osmotic flow. We use the Cartesian (x,y) coordinate with its origin at the bottom of the channel. Figure 1 depicts the geometry and the coordinate system. The light dashed lines denote the computational domain, which is periodic in the flow direction. Notice that the EO flow is symmetric with respect to the centerline of the channel (thick dashed line).

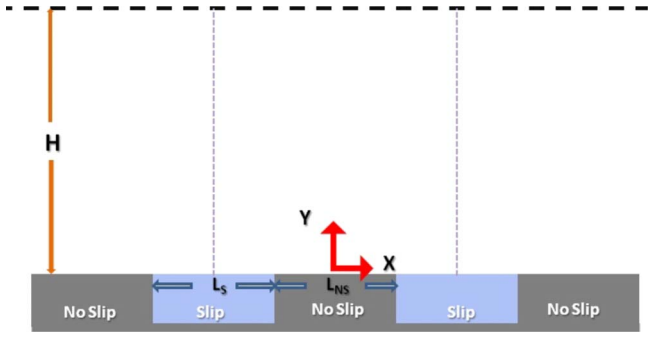

FIG. 1. (Color online) A schematic of a superhydrophobic surface and the coordinate system where $H=L_S+L_{NS}$ and the double layer thickness $\lambda_D \ll H$.

Since the Reynolds number associated with electrokinetic flows is typically small, flow velocities $\vec{u}$ satisfy the Stokes equation

$$-\nabla p - \frac{1}{2\lambda_D^2}(C_+ - C_-)\nabla\varphi + \nabla^2\vec{u} = 0. \tag{1}$$

The fluid is incompressible,

$$\nabla \cdot \vec{u} = 0. \tag{2}$$

In the above, all the variables are dimensionless. Various scales used in the normalization scheme will be specified later. p is the pressure; C is the ion's concentration; the subscripts (+) and (−) denote, respectively, the cations and the anions; φ is the electric potential; $\vec{E}=-\nabla\varphi$ is the electric field; $\lambda_D=[1/(L_{NS}^*+L_S^*)]\sqrt{\varepsilon_1^* R^* T^*/2F^{*2}C_0^*}$ is the dimensionless Debye screening length normalized with the length of the periodic cell $L_{NS}^*+L_S^*$; C_0^* is the solute's bulk concentration; R^* is the ideal gas constant; F^* is the Faraday constant; and T^* is the temperature.

The electric potential φ obeys the Poisson equation

$$\nabla^2\varphi = -\frac{C_+ - C_-}{2\lambda_D^2}. \tag{3}$$

The ions' fluxes,

$$\vec{N}_\pm = -D_\pm \nabla C_\pm - z_\pm D_\pm C_\pm \nabla\varphi + mC_\pm\vec{u}, \tag{4}$$

satisfy the Nernst-Planck equations

$$\nabla \cdot \vec{N}_\pm = 0. \tag{5}$$

In the above, $m=\varepsilon_1^* R^{*2}T^{*2}/\mu^* D_+^* F^{*2}$ is the ionic drag coefficient and μ^* is the solvent's dynamic viscosity. Further we use $L_{NS}^*+L_S^*$ as the length scale, R^*T^*/F^* as the electric potential scale, $\varepsilon_1^* R^{*2}T^{*2}/[\mu^* F^{*2}(L_{NS}^*+L_S^*)]$ as the velocity scale, the bulk concentration C_0^* as the concentration scale, $\varepsilon_1^* R^{*2}T^{*2}/[F^{*2}(L_{NS}^*+L_S^*)^2]$ as the pressure scale, and $D_\pm = D_\pm^*/D_+^*$ is the ratio of the molecular diffusivities (i.e., $D_+ = 1$). Below, for simplicity, we will assume $D_+=D_-$ (it is straightforward to extend to the case of $D_+ \neq D_-$). Boundary conditions will be specified later.

III. PERTURBATION EXPANSION IN TERMS OF THE APPLIED ELECTRIC FIELD'S INTENSITY

Here, we assume that the applied electric field is much smaller than the electric field induced by the surface charge. In other words, the external electric field only slightly disturbs the electric potential and the ions' concentration of the equilibrium double layer. Under these conditions, one can use a regular perturbation expansion around the equilibrium double layer,

$$\begin{pmatrix} \varphi \\ C_{\pm} \\ \vec{u} \end{pmatrix} = \begin{pmatrix} \varphi^{(0)} \\ C_{\pm}^{(0)} \\ 0 \end{pmatrix} + \delta \begin{pmatrix} \varphi^{(1)} \\ C_{\pm}^{(1)} \\ \vec{u}^{(1)} \end{pmatrix} + O(\delta^2). \tag{6}$$

In the above, we denoted the perturbed quantities with the prefix δ that is the ratio between the magnitudes of the external electric field and that of the equilibrium electric double layer $(E_0\lambda_D/\zeta)$.

A. Zeroth-order approximation

We assume that $\varphi^{(0)}$ and $C_{\pm}^{(0)}$ are, respectively, the equilibrium electric potential and the equilibrium concentrations induced by surface charges in the absence of an external electric field. At equilibrium, ions' concentrations $C_{\pm}^{(0)}$ obey the classical Boltzmann distribution

$$C_{\pm}^{(0)} = e^{\mp\varphi^{(0)}}. \tag{7}$$

The electric potential $\varphi^{(0)}$ satisfies the Poisson-Boltzmann equation

$$\nabla^2\varphi^{(0)} = \frac{\sinh(\varphi^{(0)})}{\lambda_D^2}. \tag{8}$$

The boundary conditions are $\varphi_1^{(0)}=\zeta_{NS}$ on the liquid-solid interface, $\varphi_1^{(0)}=\zeta_S$ on the liquid-gas interface, and $\varphi_1^{(0)}=0$ at the center of the channel. Periodic boundary conditions are imposed along the x direction. Here, we assume that the height of the channel is much larger than the double layer thickness $(H \gg \lambda_D)$ (thin-double-layer limit). To approximate discontinuities in zeta potentials of no-slip and no-shear regions, we use the smooth Heaviside function H, which remains zero within the no-slip region and one within the no-shear region,

$$H = \begin{cases} 1, & s > h \\ 0, & s < -h \\ \frac{1}{2}\left[1 + \frac{s}{h} + \frac{1}{\pi}\sin\left(\frac{\pi s}{h}\right)\right], & |s| < h, \end{cases} \tag{9}$$

where $s=|x|-1/4$ and $h=0.005$.

B. First-order approximation

The external electric field slightly perturbs the equilibrium electric double layer. The first-order equations $O(\delta)$ are linear in terms of the perturbed quantities. The first-order electric potential is not periodic along the x direction in the presence of the external electric field. But the electric field intensities $\vec{E}=-\nabla\varphi$ remain periodic along the flow direction. To facilitate computation, we will directly solve the electric field intensities $[\vec{E}=(E_x,E_y)]$ rather than the electric potential. The equations of $\vec{E}=(E_x,E_y)$ can be readily derived by differentiating the Poisson equation (3), respectively.

Substituting series (6) into Eqs. (1)–(5), retaining terms up to $O(\delta)$, we have

$$-\nabla p^{(1)} - \frac{1}{2\lambda_D^2}[-(C_+^{(0)} - C_-^{(0)})\vec{E}^{(1)} + (C_+^{(1)} - C_-^{(1)})\nabla\varphi^{(0)}] + \nabla^2\vec{u}^{(1)} = 0, \tag{10}$$

$$\nabla \cdot \vec{u}^{(1)} = 0, \tag{11}$$

$$\nabla^2\vec{E}^{(1)} = \frac{\nabla C_+^{(1)} - \nabla C_-^{(1)}}{2\lambda_D^2}, \tag{12}$$

$$\nabla \cdot [-\nabla C_{\pm}^{(1)} - z_{\pm}(-C_{\pm}^{(0)}\vec{E}^{(1)} + C_{\pm}^{(1)}\nabla\varphi^{(0)}) + mC_{\pm}^{(0)}\vec{u}^{(1)}] = 0. \tag{13}$$

At the channel's wall $(y=0)$, we assume that the permittivity of the surface is much smaller than that of the liquid. Thus, the electric insulated condition can be imposed,

$$E_y^{(1)} = -\frac{\partial\varphi^{(1)}}{\partial n} = 0, \quad \text{at } y = 0. \tag{14}$$

Notice that $\partial E_x^{(1)}/\partial y = -\partial^2\varphi^{(1)}/\partial y\,\partial x = -\partial^2\varphi^{(1)}/\partial x\,\partial y = \partial E_y^{(1)}/\partial x$ and $E_y^{(1)}=0$ at $y=0$. The boundary condition of $E_x^{(1)}$ can be expressed as

$$\frac{\partial E_x^{(1)}}{\partial y} = 0, \quad \text{at } y = 0. \tag{15}$$

With respect to ions' concentrations, the zero-flux conditions are imposed,

$$-\frac{\partial C_{\pm}^{(1)}}{\partial y} - z_{\pm}\left(-C_{\pm}^{(0)}E_y^{(1)} + C_{\pm}^{(1)}\frac{\partial\varphi^{(0)}}{\partial y}\right) = 0, \quad \text{at } y = 0. \tag{16}$$

The velocities at the no-slip region obey the no-slip condition

$$u^{(1)} = 0, \quad v^{(1)} = 0. \tag{17}$$

At the no-shear region they satisfy the perfect-slip condition

$$\frac{\partial u^{(1)}}{\partial y} = 0, \quad v^{(1)} = 0. \tag{18}$$

At the center of the channel, the symmetric conditions are imposed for the velocities, the ionic concentrations, as well as the pressure. The electric field intensities are, respectively, given by

$$E_x^{(1)} = E_0, \quad E_y^{(1)} = 0. \tag{19}$$

Along the flow direction, the periodic condition $A[-(L_{ns}+L_s)/2]=A[(L_{ns}+L_s)/2]$ is satisfied, where A stands for any variable including the velocities, the pressure, the electric field intensities, and the ions' concentrations.

To examine the enhancement of EO flows over a superhydrophobic surface, the averaged velocity can be computed by integrating the velocity along any cross section. Here, we choose the cross section at $x=0$. Because the averaged velocity is proportional to the external electric field, we can further define an averaged electro-osmotic mobility to characterize EO flows:

$$U_a = \frac{\int_0^H u dy}{HE_0}. \tag{20}$$

To study the possibility of the enhancement due to the slip, the averaged EO mobility U_a will be compared against that of a uniformly charged no-slip surface.

IV. SOLUTION PROCEDURE AND CODE VERIFICATION

The zeroth-order and first-order equations with corresponding boundary conditions were solved with the finite element software COMSOL 3.5 (Comsol™, Sweden). In order to resolve the detailed structure of the electric double layer and capture the discontinuities in zeta potentials and slip and no-slip conditions in the proximity of the gas-solid interface, nonuniform elements were used with dense mesh concentrated next to the surface and the elements' size gradually increased as the distance from the surface increased. The mesh was refined a few times to assure that the computational results are mesh independent.

To verify our numerical algorithm, we computed the averaged EO mobility in the case of low zeta potentials and compared our numerical results with analytical solutions reported by Squires [46] and Bahga *et al.* [47]. Under the assumptions of small zeta potentials ($|\zeta| \ll 1$) and the thin-double-layer limit, the averaged EO mobility is expressed as [46,47]

$$U_a = -[\zeta_{NS} + (\beta/\lambda_D)\zeta_S], \tag{21}$$

where β is the effective hydrodynamic slip length and is deduced from the increase in the flow rate of a pressure-driven flow due to the slip over the same superhydrophobic surface. For the conditions given here, $\beta=0.0552$. Detailed calculation of β is presented in the Appendix.

Interestingly, for an uncharged liquid-gas interface, Eq. (21) indicates that the averaged EO mobility U_a is equal to $-\zeta_{NS}$. No enhancement of EO flows is predicted. The same observation was also made by Squires [46] using the Lorentz reciprocal theorem, wherein he explained that the EO flow appears to slip over the charged region without experiencing any shear force from the no-shear region.

Figure 2 plots the averaged EO mobility U_a as a function of $|\zeta_{NS}|$ when $\lambda_D=0.01$ and the liquid-gas interface is uncharged. The line and the symbols correspond, respectively, to the averaged EO mobility predicted by Eq. (21) and the one computed by numerical simulations. Our numerical simulations agreed well with Eq. (21) when $|\zeta_{NS}|<1$. Since Eq. (21) is derived in the limit of low zeta potentials, it is not surprising that in the case of $|\zeta_{NS}|>1$ the computed U_a deviates from theoretical predictions.

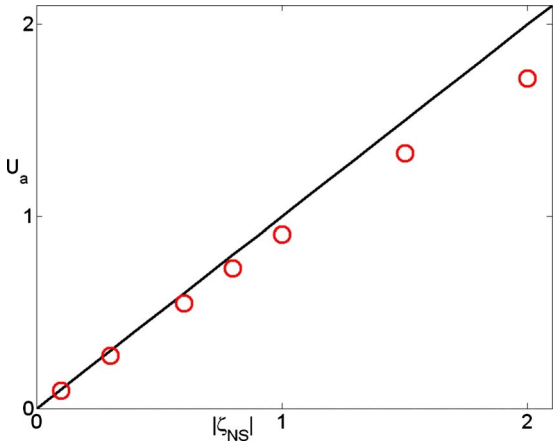

FIG. 2. (Color online) The averaged EO mobility U_a as a function of $|\zeta_{NS}|$ when $\lambda_D=0.01$ and the liquid-gas interface is uncharged. The line and the symbols correspond, respectively, to the averaged EO mobility predicted by Eq. (21) and that computed by numerical simulations.

In addition, Fig. 3 depicts the averaged EO mobility U_a as a function of ζ_S/ζ_{NS}, the ratio of zeta potentials of the liquid-gas and liquid-solid interfaces when $\lambda_D=0.01$ and $\zeta_{NS}=-0.1$. Once again, our simulations are in excellent agreements with theoretical predictions.

In the case of a uniformly charged superhydrophobic surface ($\zeta_S=\zeta_{NS}$), Bahga *et al.* [47] demonstrated that Eq. (21) is indeed applicable for an arbitrary double layer thickness assuming that the zeta potential remains small ($|\zeta| \ll 1$). Figure 4 plots the averaged EO mobility U_a as a function of $1/\lambda_D$ when $\zeta_S=\zeta_{NS}=-0.1$. Our simulations agreed well with Eq. (21) over a broad range of double layer lengths. The excellent agreements with Eq. (21) verified our numerical code. Next we can compute the averaged EO mobility in the case of $|\zeta_{NS}|>1$ where Eq. (21) fails.

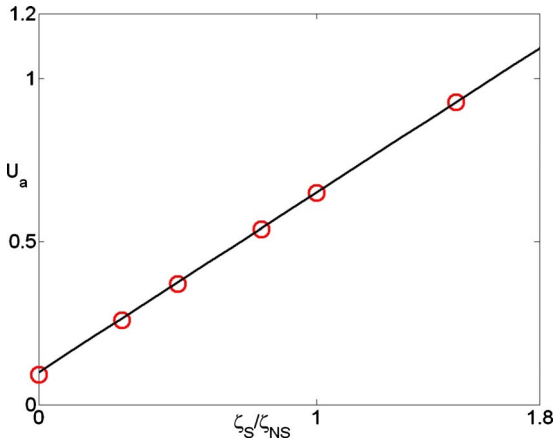

FIG. 3. (Color online) The averaged EO mobility U_a as a function of ζ_S/ζ_{NS}, the ratio between the zeta potentials of liquid-gas and liquid-solid interfaces when $\lambda_D=0.01$ and $\zeta_{NS}=-0.1$. The line and the symbols correspond, respectively, to the averaged EO mobility predicted by Eq. (21) and that computed by numerical simulations.

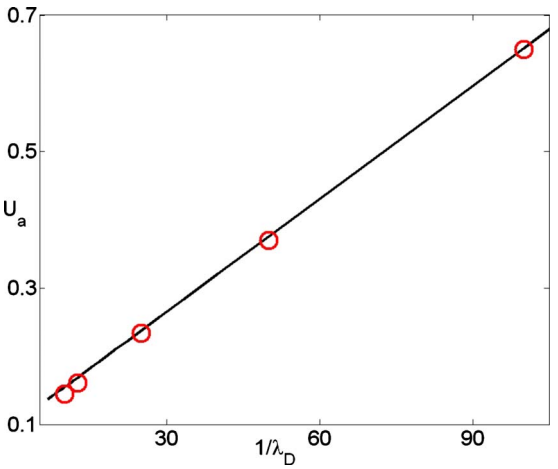

FIG. 4. (Color online) The averaged EO mobility U_a as a function of $1/\lambda_D$, when $\zeta_S=-0.1$ and $\zeta_{NS}=-0.1$. The line and the symbols correspond, respectively, to the averaged EO mobility predicted by Eq. (21) and that computed by numerical simulations.

V. RESULTS AND DISCUSSION

Figure 5 depicts the averaged EO mobility U_a as a function of $|\zeta_{NS}|$ when $\lambda_D=0.03$. The dashed and dashed-dotted lines with symbols correspond, respectively, to $\zeta_S/\zeta_{NS}=0$ and $\zeta_S/\zeta_{NS}=1$. For comparison, the solid line represents the EO mobility of the surface which is of no slip and is homogeneously charged. In contrast to the results presented in Sec. IV, when $|\zeta_{NS}|>1$, the averaged EO mobility over a superhydrophobic surface with uncharged liquid-gas interfaces, is much smaller than the one over the homogeneously charged no-slip surface. When liquid-gas interfaces are charged, the EO mobility is amplified much less than their counterpart of low zeta potentials.

The above phenomena are readily explained: the external electric field drives excess ions inside the double layer to migrate and induces an EO flow that simultaneously transports ions inside the double layer. The processes of ion migration and convection lead to surface conduction. Consider that liquid-solid and liquid-gas interfaces normally have different surface properties. Likely the surface conduction over the entire surface is not homogeneous. In particular, it might become discontinuous in the proximity of the gas-solid interface. In order to guarantee the conservation of the electric current, ions must enter the electric double layer from the bulk when the surface conduction increases [at left in Fig. 6(a)]. Ions must be depleted into the bulk from the double layer when the surface conduction decreases [at right in Fig. 6(a)]. In turn, this depletion-accumulation process deforms the electric field to penetrate the double layer, thus weakening the tangential component of the electric field that is responsible to drive the EO flow. This process leads to a smaller EO mobility in comparison to Eq. (21), where the external electric field is assumed to be parallel to the surface. As the zeta potential grows larger, the tangential component of the electric field becomes weaker, in order to maintain the global ion conservation. Moreover, this depletion-accumulation process also creates a bulk concentration gradient outside the double layer. For instance, at left in Fig. 6(a), the penetrated electric field attracts counterions into the double layer and repels coions, creating a salt sink outside the double layer. On the contrary, at right in Fig. 6(a), the electric field creates a salt source. It is well known that the concentration gradient can induce a diffusio-osmotic flow [49] that might complicate the EO flow. Its effect will be discussed later.

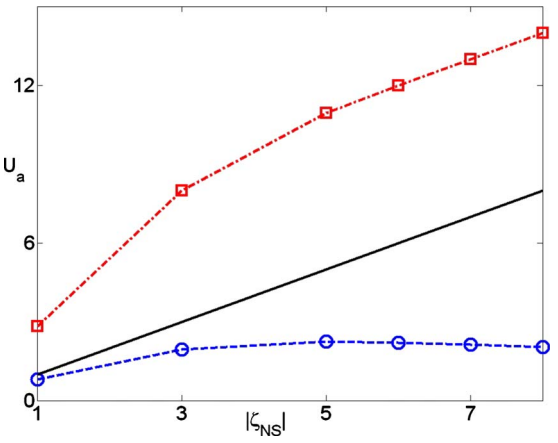

FIG. 5. (Color online) The averaged EO mobility U_a as a function of $|\zeta_{NS}|$ when $\lambda_D=0.03$. The dashed and dashed-dotted lines with symbols correspond, respectively, to $\zeta_S/\zeta_{NS}=0$ and $\zeta_S/\zeta_{NS}=1$. The solid line represents the EO mobility of a homogeneously charged nonslip surface.

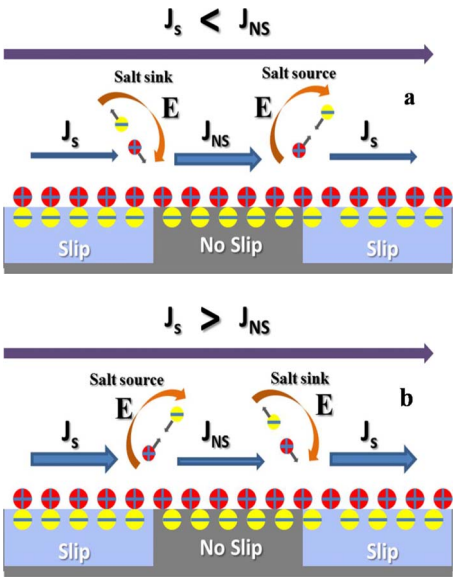

FIG. 6. (Color online) A schematic of nonuniform surface conduction over a superhydrophobic surface and its effects on deforming the electric field and bulk concentration. (a) The surface current inside the double layer of the no-slip region is larger than that of the no-shear region ($J_{NS}>J_S$). (b) The surface current inside the double layer of the no-slip region is smaller than that of the no-shear region ($J_{NS}<J_S$).

In the case of $\zeta_S/\zeta_{NS}=1$, since there is no shear resistance at the liquid-gas interface, the EO flow inside the double layer near the no-shear region is significantly boosted, resulting in a higher surface conduction compared to that near the

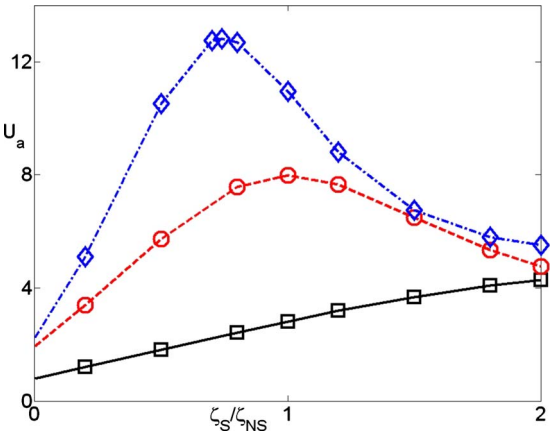

FIG. 7. (Color online) The averaged EO mobility U_a as a function of ζ_S/ζ_{NS} when $\lambda_D=0.03$. The solid, dashed, and dashed-dotted lines with symbols correspond, respectively, to $\zeta_{NS}=-1$, $\zeta_{NS}=-3$, and $\zeta_{NS}=-5$.

no-slip region. The conservation of the current requires that, as the electric field penetrates the double layer, ions are depleted into the bulk from the double layer at left in Fig. 6(b) and are withdrawn into the double layer at right in Fig. 6(b). Similarly this depletion-accumulation process results in a reduction in the tangential component of the electric field and thus a reduction in the EO mobility. Meanwhile, a salt sink and a salt source are created. This bulk concentration gradient, in turn, induces a diffusio-osmotic flow.

Consider the following scenario: in the case of $|\zeta_S| < |\zeta_{NS}|$, the migration current over the no-shear region is normally smaller than that over the no-slip region. But the hydrodynamic slip at the no-shear region typically increases the convection current. Thus, it is possible that there exists a critical ζ_S/ζ_{NS} where the surface current having both migration and convection components may become homogenous again in the proximity of the gas-solid interface. In other words, the electric field is likely again parallel to the surface, and thus a maximum EO mobility will be anticipated.

To confirm our speculation, Fig. 7 depicts the averaged EO mobility U_a as a function of ζ_S/ζ_{NS} when $\lambda_D=0.03$. The solid, dashed, and dashed-dotted lines with symbols correspond, respectively, to $\zeta_{NS}=-1$, $\zeta_{NS}=-3$, and $\zeta_{NS}=-5$. In the case of $\zeta_{NS}=-1$, as ζ_S/ζ_{NS} increases, the averaged EO mobility also increases since the surface conduction over the superhydrophobic surface is small, and the effect of the nonuniform surface conduction is inappreciable. In contrast, when $\zeta_{NS}=-3$ and $\zeta_{NS}=-5$, the EO mobility U_a initially increases, reaches a maximum, and then decreases as ζ_S/ζ_{NS} increases. In the case of $\zeta_{NS}=-5$, the maximum EO mobility is predicted around $\zeta_S/\zeta_{NS}=0.74$.

Figure 8 plots the electric field lines for $\zeta_S/\zeta_{NS}=0.5$ [Fig. 8(a)], $\zeta_S/\zeta_{NS}=0.74$ [Fig. 8(b)], and $\zeta_S/\zeta_{NS}=1$ [Fig. 8(c)] when $\lambda_D=0.03$ and $\zeta_{NS}=-5$. The arrows indicate the direction of the electric field in the proximity of the gas-solid interface. The background is the local salt concentration $C^{(1)}=(C_+^{(1)}+C_-^{(1)})/2$. Figure 8 is consistent with our intuitive argument. For instance, when $\zeta_S/\zeta_{NS}=0.5$, the surface conduction over the no-slip region is larger than that over the no-shear region. Thus, ions enter the double layer at the left

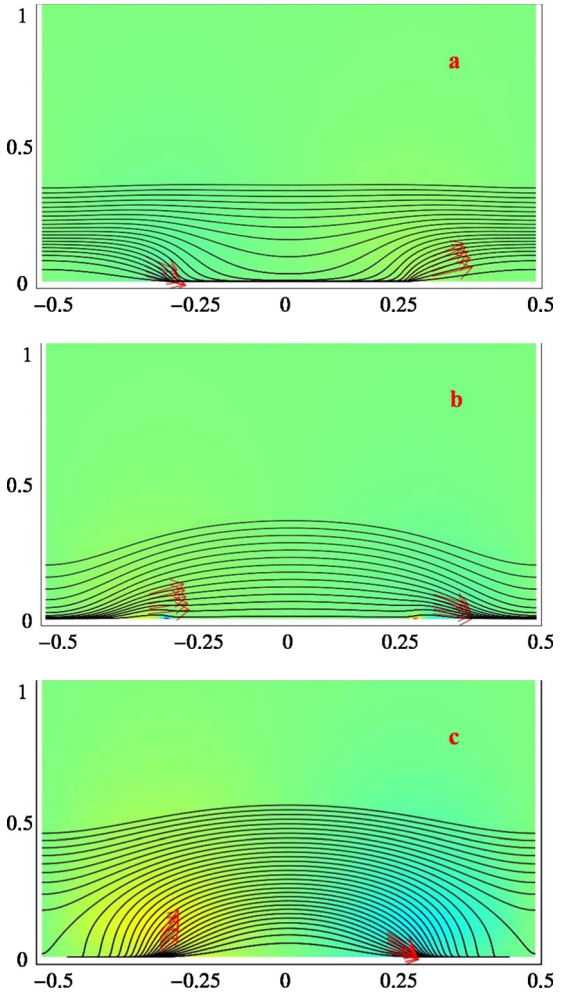

FIG. 8. (Color online) The electric field lines for (a) $\zeta_S/\zeta_{NS}=0.5$, (b) $\zeta_S/\zeta_{NS}=0.74$, and (c) $\zeta_S/\zeta_{NS}=1$, when $\lambda_D=0.03$ and $\zeta_{NS}=-5$. The arrows indicate the direction of the electric field. The background color is the local salt concentration.

and are depleted into the bulk at the right to maintain the conversation of the current. Accordingly, the electric field points into the double layer at the left and points outward at the right. In the case of $\zeta_S/\zeta_{NS}=1$, the surface conduction over the no-shear region exceeds that over the no-slip region and the direction of the electric field is reversed. In contrast, when $\zeta_S/\zeta_{NS}=0.74$, the difference of ions' migrations inside the double layer, between the no-shear and no-slip regions, caused by different zeta potentials is offset by the difference of convections due to the slip. The surface conduction is nearly homogenous in the proximity of the gas-solid interface. Accordingly, the electric field is nearly parallel to the surface or the tangential component of the electric field increases. Therefore, the EO flow reaches its maximum.

As discussed earlier, the nonuniform surface conduction over a superhydrophobic surface not only weakens the tangential component of the electric field, but also creates a bulk concentration gradient outside the double layer. Figure 9 plots the local salt concentration $C^{(1)}=(C_+^{(1)}+C_-^{(1)})/2$ as a function of x when $\lambda_D=0.03$ and $y=0.1$ (outside the double layer). The solid, dashed, and dashed-dotted lines correspond, respectively, to $\zeta_S/\zeta_{NS}=0.5$, $\zeta_S/\zeta_{NS}=0.74$, and

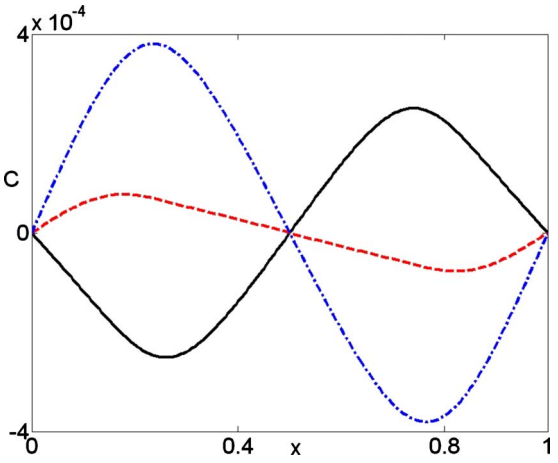

FIG. 9. (Color online) The local salt concentration $C^{(1)}=(C_+^{(1)}+C_-^{(1)})/2$ as a function of x when $\lambda_D=0.03$, $\zeta_{NS}=-5$, and $y=0.1$. The solid, dashed, and dashed-dotted lines correspond, respectively, to $\zeta_S/\zeta_{NS}=0.5$, $\zeta_S/\zeta_{NS}=0.74$, and $\zeta_S/\zeta_{NS}=1$.

$\zeta_S/\zeta_{NS}=1$. Consistent with Fig. 8, when $\zeta_S/\zeta_{NS}=0.5$, a salt sink is created to the left of the no-slip region and a salt source is created to the right of the no-slip region. In contrast, when $\zeta_S/\zeta_{NS}=1$, the salt source and salt sink locate at the left and at the right, respectively. In the case of $\zeta_S/\zeta_{NS}=0.74$, the concentration gradient is the smallest since the surface conduction is nearly homogeneous.

The bulk concentration gradient induces a diffusio-osmotic flow that drives liquid from the region of high concentration to that of low concentration. In the case of $\zeta_S/\zeta_{NS}=0.5$, the diffusio-osmotic flow is opposite to the EO flow and weakens the EO flow. When $\zeta_S/\zeta_{NS}=1$, the diffusio-osmotic flow is along the same direction of the EO flow, potentially enhancing the EO flow. However, Fig. 7 suggests a different story that can be explained. At large ζ_S/ζ_{NS}, the loss of the EO flow caused by the weaker tangential electric field component exceeds the gain of the EO flow due to the diffusio-osmotic flow. In other words, the effect of the diffusio-osmotic flow on enhancing EO flows is secondary.

VI. CONCLUSION

We numerically studied electro-osmotic flows under the action of an electric field over a patterned superhydrophobic surface with periodically distributed regions of no shear and no slip. Our numerical simulations were in excellent agreements with theoretical predictions in the limit of low surface's zeta potentials [46,47]. Significant enhancement of EO flows can be achieved only when the liquid-gas interface is charged. When surface's zeta potentials are large, nonuniform surface conduction due to the mismatch of ions' migration and convection over no-shear and no-slip regions cause the electric field to penetrate the double layer to maintain the conservation of the current. Such an action leads to a reduction in the tangential component of the electric field inside the double layer responsible for driving EO flows. Therefore, the enhancement of EO flows due to the slip is much smaller than that predicted by the theoretical model without accounting for the nonuniform surface conduction. Under certain conditions, the enhancement of EO flows due to the slip might be potentially lost in comparison with EO flows over a homogeneously charged no-slip surface.

Our results indicate that one must be careful to choose superhydrophobic surfaces for potential electrokinetic applications since the enhancement of EO flows may not always exist, in particular, for moderately or highly charged surfaces. In order to fully exploit the advantages of a superhydrophobic surface, the surface charge on the liquid-solid interface has to be judiciously chosen to maximize the enhancement of EO flows. In other words, it is not always beneficial to replace a homogeneously charged no-slip surface with a superhydrophobic surface.

A superhydrophobic surface is covered with microstructures or nanostructures such as grooves. This roughness traps gas bubbles inside the textured structures and prevents liquids from wetting the grooves, providing a way to reduce the friction. In the paper, our model assumed that the liquid-gas interface is flat and of no shear. Detailed justification of these assumptions has been presented by Ybert *et al.* [27]. Briefly, when surfaces with roughness are made of grooves (Fig. 1), and the viscosity of the gas is much smaller than that of the liquid, the curvature effect and the finite dissipation within the gas phase are not important [27].

Finally, in our results, we assumed that the liquid-gas interface carries charges. There are experiments and molecular-dynamics simulations supporting that the water-air interface is negatively charged due to excess OH^- [52,53]. The zeta potential of the water-air interface was measured to be −65 mV [54,55].

ACKNOWLEDGMENT

I thank the referees for helpful comments and directing Ref. [49] into my attention.

APPENDIX

In this appendix, we solve a pressure-driven flow over a periodical array of slip-stick strips in a two-dimensional channel. To calculate the flow field, we define a stream function $\psi(x,y)$ by

$$u=\frac{\partial\psi}{\partial y},\quad v=-\frac{\partial\psi}{\partial x}. \tag{A1}$$

To facilitate the derivation, one can decompose this linear Stokes's problem into a superposition of a parabolic flow and a perturbation to the parabolic flow,

$$\psi(x,y)=\psi_P(y)+\tilde{\psi}(x,y),\quad \psi_P(y)=y^2-\frac{y^3}{3}. \tag{A2}$$

In the above, we use the length of the periodic cell $L_{NS}^*+L_S^*$ as the length scale and $-\{1/[2\mu^*(L_{NS}^*+L_S^*)^2]\}(dP^*/dx^*)$ as the velocity scale to nondimensionalize Eq. (A2).

The boundary conditions for $\tilde{\psi}$ over the superhydrophobic surface are

$$\tilde{\psi} = 0, \quad \text{at } y = 0, \tag{A3}$$

$$\frac{\partial \tilde{\psi}}{\partial y} = 0, \quad \text{at } y = 0, \ |x| \le 1/4 \ \text{(no-slip region)}, \tag{A4}$$

$$2 + \frac{\partial^2 \tilde{\psi}}{\partial y^2} = 0, \quad \text{at } y = 0, \ 1/4 < |x| \le 1/2 \ \text{(no-shear region)}. \tag{A5}$$

At the center of the channel, symmetric conditions are satisfied,

$$\frac{\partial^2 \tilde{\psi}}{\partial y^2} = 0, \quad \frac{\partial \tilde{\psi}}{\partial x} = 0, \quad \text{at } y = 1. \tag{A6}$$

Here, we assume that the height of the channel is equal to $2(L_{NS}^* + L_S^*)$.

To determine the stream function, we can first calculate the perturbation vorticity $\tilde{\omega}$ since the stream function satisfies

$$\frac{\partial^2 \tilde{\psi}}{\partial x^2} + \frac{\partial^2 \tilde{\psi}}{\partial y^2} = \tilde{\omega}. \tag{A7}$$

The equation of the perturbation vorticity $\tilde{\omega}$ can be obtained by taking the curl of the Stokes equation,

$$\frac{\partial^2 \tilde{\omega}}{\partial x^2} + \frac{\partial^2 \tilde{\omega}}{\partial y^2} = 0. \tag{A8}$$

The solution of Eq. (A8) can be found by using separation of variables,

$$\tilde{\omega} = \sum_{n=1}^{\infty} a_n \cos \lambda_n x (e^{-\lambda_n y} - e^{-2\lambda_n} e^{\lambda_n y}), \tag{A9}$$

where $\lambda_n = 2n\pi$. Accounting for the symmetry, we have used the condition $\tilde{\omega} = 0$ at the center ($y = 1$) to derive Eq. (A9).

With $\tilde{\omega}$, the stream function can thus be expressed using the separation of variables as

$$\tilde{\psi} = a_0 y + b_0 + \sum_{n=1}^{\infty} f_n(y) \cos \lambda_n x. \tag{A10}$$

By substituting Eq. (A10) into Eq. (A7), one can obtain

$$f_n'' - \lambda_n^2 f_n = a_n (e^{-\lambda_n y} - e^{-2\lambda_n} e^{\lambda_n y}). \tag{A11}$$

With boundary conditions (A3) and (A6), the perturbation stream function $\tilde{\psi}$ is therefore given by

$$\tilde{\psi} = a_0 y + \sum_{n=1}^{\infty} \frac{a_n}{2\lambda_n} (y e^{-\lambda_n y} - y e^{-2\lambda n} e^{\lambda_n y}) \cos \lambda_n x. \tag{A12}$$

Based on the definition of the effective slip length β [24], the additional flow rate due to the slip can be written as $\tilde{Q} = Q - 4/3 = 4\beta$. Since

$$\tilde{Q} = 2 \int_0^1 \tilde{u} dy = 2\tilde{\psi}(1) = 2a_0, \tag{A13}$$

one can immediately obtain $\beta = a_0/2$.

To obtain the slip length, one needs to calculate the set of coefficients a_n. The coefficients will be determined by the boundary conditions (A4) on the no-slip region and Eq. (A5) on the no-shear region. Dual series equations for the coefficients a_n are inferred as

$$a_0 + \sum_{n=1}^{\infty} a_n \frac{1 - e^{-2\lambda n}}{2\lambda_n} \cos \lambda_n x = 0, \quad \text{for } |x| \le 1/4, \tag{A14}$$

$$2 + \sum_{n=1}^{\infty} - a_n (1 + e^{-2\lambda n}) \cos \lambda_n x = 0, \quad \text{for } 1/4 < |x| \le 1/2. \tag{A15}$$

The dual series Eqs. (A14) and (A15) do not have a standard analytical form [56] and have to be solved numerically.

To calculate coefficients a_n, we truncate the dual series equation at a_{N-1}, multiply $\cos 2m\pi x$ ($m < N$) with Eqs. (A14) and (A15), and integrate them along their respective domains. We have

$$a_0 \int_{-1/4}^{1/4} \cos 2m\pi x dx + \sum_{n=1}^{\infty} a_n \int_{-1/4}^{1/4} \frac{1 - e^{-2\lambda_n}}{2\lambda_n} \times \cos 2m\pi x \cos \lambda_n x dx = 0, \tag{A16}$$

$$4 \int_{1/4}^{1/2} \cos 2m\pi x dx - \sum_{n=1}^{\infty} 2a_n \int_{1/4}^{1/2} (1 + e^{-2\lambda_n}) \times \cos 2m\pi x \cos \lambda_n x dx = 0. \tag{A17}$$

Adding Eqs. (A16) and (A17) together, the result can be written as a linear system of equations:

$$\sum_{n=0}^{N-1} A_{mn} a_n = B_m, \tag{A18}$$

where

$$A_{0n} = \int_{-1/4}^{1/4} \cos 2m\pi x dx, \tag{A19}$$

$$A_{mn} = \int_{-1/4}^{1/4} \frac{1 - e^{-2\lambda_n}}{2\lambda_n} \cos 2m\pi x \cos \lambda_n x dx - 2\int_{1/4}^{1/2} (1 + e^{-2\lambda_n}) \cos 2m\pi x \cos \lambda_n x dx \quad (n \geq 1), \tag{A20}$$

$$B_m = -4\int_{1/4}^{1/2} \cos 2m\pi x dx. \tag{A21}$$

The resulting linear system is then solved and the solution converges upon truncation refinement.

[1] D. Lasne, A. Maali, Y. Amarouchene, L. Cognet, B. Lounis, and H. Kellay, Phys. Rev. Lett. **100**, 214502 (2008).
[2] E. Lauga, M. P. Brenner, and H. A. Stone, *Handbook of Experimental Fluid Dynamics* (Springer, New York, 2007), Chap. 19, pp. 1219–1240.
[3] A. Maali and B. Bhushan, Phys. Rev. E **78**, 027302 (2008).
[4] C. Neto, D. R. Evans, E. Bonaccurso, H. J. Butt, and V. S. J. Craig, Rep. Prog. Phys. **68**, 2859 (2005).
[5] U. Ulmanella and C. M. Ho, Phys. Fluids **20**, 101512 (2008).
[6] O. Vinogradova, Int. J. Min. Process. **56**, 31 (1999).
[7] Y. Wang, B. Bhushan, and A. Maali, J. Vac. Sci. Technol. A **27**, 754 (2009).
[8] L. Bocquet and J. Barrat, Soft Matter **3**, 685 (2007).
[9] O. I. Vinogradova, Langmuir **11**, 2213 (1995).
[10] W. Barthlott and C. Neinhuis, Planta **202**, 1 (1997).
[11] J. P. Rothstein, Annu. Rev. Fluid Mech. **42**, 89 (2010).
[12] D. C. Tretheway and C. D. Meinhart, Phys. Fluids **14**, L9 (2002).
[13] J. Ou, B. Perot, and J. P. Rothstein, Phys. Fluids **16**, 4635 (2004).
[14] J. Ou and J. P. Rothstein, Phys. Fluids **17**, 103606 (2005).
[15] C. Lee, C. H. Choi, and Chang-Jin CJ Kim, Phys. Rev. Lett. **101**, 064501 (2008).
[16] M. Z. Bazant and O. I. Vinogradova, J. Fluid Mech. **613**, 125 (2008).
[17] D. Byun, J. Kim, H. S. Ko, and H. C. Park, Phys. Fluids **20**, 113601 (2008).
[18] C. H. Choi and C. J. Kim, Phys. Rev. Lett. **96**, 066001 (2006).
[19] C. H. Choi, U. Ulmanella, J. Kim, C. M. Ho, and C. J. Kim, Phys. Fluids **18**, 087105 (2006).
[20] C. Cottin-Bizonne, J. L. Barrat, L. Bocquet, and E. Charlaix, Nature Mater. **2**, 237 (2003).
[21] J. Davies, D. Maynes, B. W. Webb, and B. Woolford, Phys. Fluids **18**, 087110 (2006).
[22] F. Feuillebois, M. Z. Bazant, and O. I. Vinogradova, Phys. Rev. Lett. **102**, 026001 (2009).
[23] P. Gao and J. J. Feng, Phys. Fluids **21**, 102102 (2009).
[24] E. Lauga and H. A. Stone, J. Fluid Mech. **489**, 55 (2003).
[25] P. Joseph, C. Cottin-Bizonne, J. M. Benoi, C. Ybert, C. Journet, P. Tabeling, and L. Bocquet, Phys. Rev. Lett. **97**, 156104 (2006).
[26] D. Maynes, K. Jeffs, B. Woolford, and B. W. Webb, Phys. Fluids **19**, 093603 (2007).
[27] C. Ybert, C. Barentin, C. Cottin-Bizonne, P. Joseph, and L. Bocquet, Phys. Fluids **19**, 123601 (2007).
[28] M. Sbragaglia and A. Prosperetti, Phys. Fluids **19**, 043603 (2007).
[29] P. Tsai, A. M. Peters, C. Pirat, M. Wessling, R. G. H. Lammertink, and D. Lohse, Phys. Fluids **21**, 112002 (2009).
[30] H. A. Stone, A. D. Stroock, and A. Ajdari, Annu. Rev. Fluid Mech. **36**, 381 (2004).
[31] T. M. Squires and S. Quake, Rev. Mod. Phys. **77**, 977 (2005).
[32] D. J. Laser and J. G. Santiago, J. Micromech. Microeng. **14**, R35 (2004).
[33] A. Ajdari and L. Bocquet, Phys. Rev. Lett. **96**, 186102 (2006).
[34] C. I. Bouzigues, P. Tabeling, and L. Bocquet, Phys. Rev. Lett. **101**, 114503 (2008).
[35] N. V. Churaev, J. Ralston, I. P. Sergeeva, and V. D. Sobolev, Adv. Colloid Interface Sci. **96**, 265 (2002).
[36] L. Joly, C. Ybert, E. Trizac, and L. Bocquet, Phys. Rev. Lett. **93**, 257805 (2004).
[37] V. M. Muller, I. P. Sergeeva, V. D. Sobolev, and N. V. Churaev, Colloid J. USSR **48**, 606 (1986).
[38] J. Eijkel, Lab Chip **7**, 299 (2007).
[39] K. Ichiki, A. E. Kobryn, and A. Kovalenko, J. Comput. Theor. Nanosci. **5**, 2004 (2008).
[40] N. J. Shirtcliffe, G. McHale, M. I. Newton, and Y. Zhang, ACS Applied Materials & Interface **1**, 1316 (2009).
[41] S. Pennathur, J. C. T. Eijkel, and A. van den Berg, Lab Chip **7**, 1234 (2007).
[42] Y. Ren and D. Stein, Nanotechnology **19**, 195707 (2008).
[43] B. A. Grimes and A. I. Liapis, J. Colloid Interface Sci. **263**, 113 (2003).
[44] A. S. Khair and T. M. Squires, Phys. Fluids **21**, 042001 (2009).
[45] H. Zhao, Phys. Fluids (to be published).
[46] T. M. Squires, Phys. Fluids **20**, 092105 (2008).
[47] S. S. Bahga, O. I. Vinogradova, and M. Z. Bazant, J. Fluid Mech. **644**, 245 (2010).
[48] A. S. Khair and T. M. Squires, Phys. Fluids **20**, 087102 (2008).
[49] J. L. Anderson, Annu. Rev. Fluid Mech. **21**, 61 (1989).
[50] J. Lyklema, *Fundamentals of Interface and Colloid Science* (Academic Press, San Diego, CA, 1995), Vol. II.
[51] R. J. Hunter, *Foundations of Colloid Science* (Oxford University Press, New York, 2001).
[52] M. Takahashi, J. Phys. Chem. B **109**, 21858 (2005).
[53] R. Zangi and Jan B. F. N. Engberts, J. Am. Chem. Soc. **127**, 2272 (2005).
[54] A. Graciaa, G. Morel, P. Saulner, J. Lachaise, and R. S. Schechter, J. Colloid Interface Sci. **172**, 131 (1995).
[55] J. S. H. Lee, I. Barbulovic-Nad, Z. Wu, X. Xuan, and D. Li, J. Appl. Phys. **99**, 054905 (2006).
[56] I. N. Sneddon, *Mixed Boundary Value Problems in Potential Theory* (North-Holland, Amsterdam, 1966).